
Nucleus Segmentation and Analysis in Breast Cancer with the MIScnn Framework

Adrian PFLEIDERER^{a,b}, Dominik MÜLLER^{a,b,1} and Frank KRAMER^a

^a*IT-Infrastructure for Translational Medical Research, University of Augsburg*

^b*Medical Data Integration Center, Institute for Digital Medicine, University Hospital Augsburg*

Abstract

The NuCLS dataset contains over 220.000 annotations of cell nuclei in breast cancers. We show how to use these data to create a multi-rater model with the MIScnn Framework to automate the analysis of cell nuclei. For the model creation, we use the widespread U-Net approach embedded in a pipeline. This pipeline provides besides the high performance convolution neural network, several preprocessor techniques and a extended data exploration. The final model is tested in the evaluation phase using a wide variety of metrics with a subsequent visualization. Finally, the results are compared and interpreted with the results of the NuCLS study. As an outlook, indications are given which are important for the future development of models in the context of cell nuclei.

1 Introduction

Analyzing nuclei from CT Slides is a difficult and repetitive task in biomedical image analysis. Therefore, more and more automated processes such as deep learning through convolutional neural networks are coming to the fore. One of the main fields of application is pathology, which focuses on the detection of tumors and other abnormalities in the context of cell nuclei. A general problem with this type of automated analysis is the limited number of sufficiently well annotated training data by experts. The large-scale NuCLS study by Amgad et al. presents an efficient method that can be used to create and verify a large amount of training data from different CT scans of cell nuclei [1]. The next big step is to show that these annotated data could be used with a standardized pipeline framework to segment and classify cell nuclei from breast tissue. In this work, we want to show that repetitive and complex tasks in a special pathology field could be efficiently and quickly automated with a deep neural network approach.

¹ Corresponding Author: Dominik Müller, IT Infrastructure for Translational Medical Research, Alter Postweg 101, 86159 Augsburg, Germany; E-mail: dominik.mueller@informatik.uni-augsburg.de

2 Methods

2.1 Data Source and Exploration

NuCLS Datasets. The raw images are provided from the Cancer Genome Atlas (TCGA) program, which is supervised by the National Cancer Institute [2] [3]. Every slide is associated with a breast cancer patient and a scan of the breast tissue. The NuCLS dataset study [1] has split down the scans into 1 mm^2 picture tiles, which capture a region of interest. They also provide for every tile a separated mask, which annotated 13 different nucleus classes. These different region classes could merge into three superclasses like tumor, stromal and sTILs because of performance and class imbalance reasons. The first channel of the mask encodes pixel-wise the label of the specific class on the tile. The instance label of each unique nucleus segmentation could be generated with the matrix product of the second and third channel. For advanced identifications the NuCLS dataset provided for every mask a separate file, in which every class instance could be identified throw coordinates. The masks were created by 25 Non-Pathologists, which are guided by supervisors. They create bounding boxes or a complete segmentation for over 220.000 nuclei. This process results in two different quality datasets. The single-rater dataset contains a large number of samples (1744), which are partially corrected and approved by the study coordinators. The multi-rater dataset (inferred P-truth) contains only 53 Samples, which are annotated separately by seven experienced Pathologists. The different masks for one sample are merged, which results in a very high quality annotation.

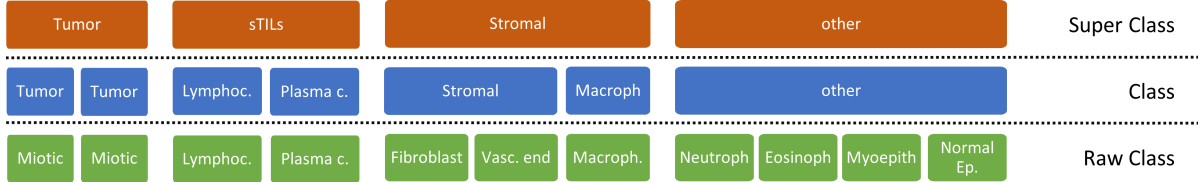


Figure 2.1: Overview over all different class partitions from raw to superclasses.

Class Distribution. The tumor, stromal, and sTILs class distribution over all samples is nearly even. All samples contain the FOV-class (field of view), which consists of any excluded classes that have not been reflected into a superclass, or all areas that have not been annotated. The "other"-superclass is the only outlier with a very small amount of samples. To strengthen the superclasses the loss function was adjusted with class weights and the "other"-class was excluded from evaluation. The NuCLS Study also excluded this class in its model training so the scores can be easily compared in the result section.

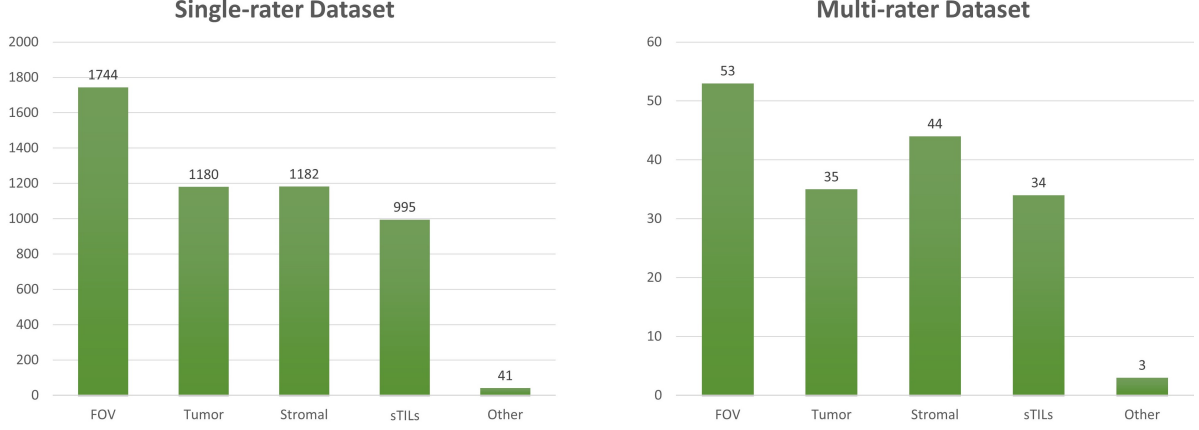


Figure 2.2: Number of samples in the dataset which contains the specific superclass. Single-rater (l). Multi-rater (r).

Exploration. Before every training phase, the data were analyzed with an exploration algorithm. These calculated the mean dimensions and the class distribution over all tiles. This information is necessary for the padding routine and class imbalanced correction later in the network configuration phase. Another routine visualizes ten randomly chosen samples to check if the mask and the tile match each other. At the end of the exploration, different partition indices are calculated for the training, validation and evaluation phases.

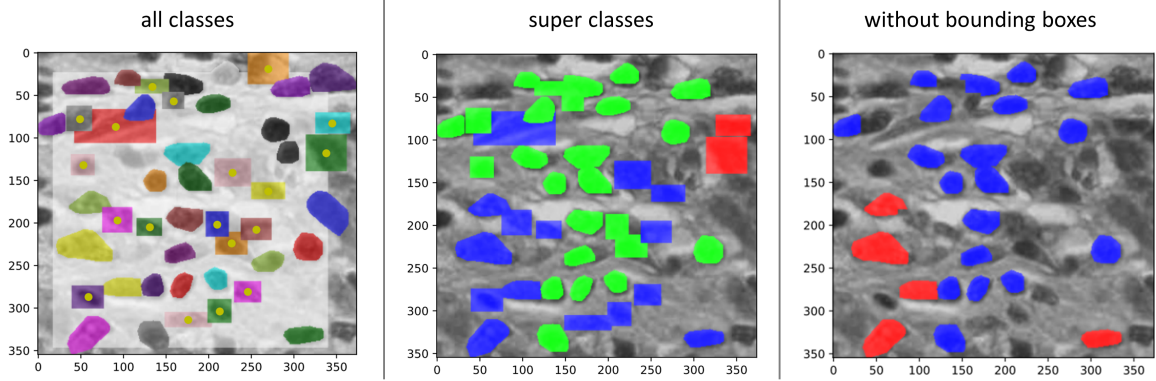


Figure 2.3: Different mask representations. All instances inclusive bounding boxes (l). Tumor, stromal and sTILs as superclasses (m). Superclass representation without bounding boxes (r).

2.2 Network and MIScnn Configurations

To create the complete network pipeline MIScnn was used [4]. MIScnn is an all-in-one python library to setup a neural network pipeline system which in turn is based on the popular TensorFlow framework [5].

2.2.1 Preprocessor

For the preprocessor phase, a customized Data-IO for the MIScnn pipeline was created. The Data-IO handles the correct data input from our images and masks. Some masks and tiles have different dimensions, therefore, the oversized image is cut down and matched to the mask. A routine has also been created to optional identify and remove bounding boxes with the corresponding localization file. Finally, the mask input and their raw classes were transformed into superclasses that delivered more examples for every segmentation class.

Network Input. Three different input datasets were created for the network. The first contains only the single-rater dataset for the training, validation and evaluation phase. The second set contains also the single-rater dataset but all bounding boxes are eliminated. Both are divided into a 60-20-20 ratio for the different phases. The last Input is a combination of the original single-rater dataset and the multi-rater dataset. Whereby the complete multi-rater dataset was used for the evaluation phase. The percentage split procedure without a fold was chosen due to hardware limitations and efficiency. The data sets are large enough, which is why possible losses in performance should be very small compared to the k-fold cross-validation procedure.

Data Augmentation. In addition to manual data manipulation, the MIScnn data augmentation functions were used to continue to enlarge the dataset. Besides color changes throw contrast, brightness, gamma and gaussian noise different transformations like scaling, elastic deform mirroring and rotation were applied. Each input into the neural network has been normalized with the z-score method, which calculates, for every pixel, the distance between the pixel value and the population mean with the unit of the standard deviation.

Patch & Padding Size. Another important aspect of the final input is the padding and patch definition. The data tiles have different sizes, which we have discussed in chapter 2.1. Tiles and masks adapted to the filter kernel are required for network input. During the data exploration, the average size over all tiles was calculated. These were used to determine the padding size, which is the nearest value in the power of 2 set. This is also the patch size for images that are larger than the average. In the context of the single-rater dataset, a mean resolution of 361 x 362 pixels was detected, resulting in a padding and patch size of 256 x 256 pixels.

2.2.2 Network Decisions

Architecture. The network is based on the effective standard U-Net adaptation from MIScnn. This standard Architecture was already successfully tested in many publications around the MIScnn framework and is widely used in the image segmentation

domain. [6] [7]

Loss-Function. A categorical focal variant of the reference function from Lin (2018) was used as the loss function, where Lin was able to achieve good results with class imbalances [8]. To counterpart the imbalanced classes the loss function needs external calculated distribution information over the whole dataset. This distribution is calculated after the balance heuristic from King and Zen (2001) [9] and further simplified by the scikit-learn framework [10]. For the single-rater dataset following class weights were generated with FOV: 0.25, Tumor: 0.37, Stromal: 0.3663 and sTILs: 0.4343.

Learning Rate. A medium-high starting value of 0.001 was used as the learning rate and decreased by a factor of 0.1 when our model reaches a plateau during training. A minimal rate of 0.00001 was defined so that the learning process remains effective. For the decrease trigger, the validation loss was monitored and a threshold from 0.0001 was specified to recognize only significant changes. After ten epochs with no significant change, the learning rate is reduced during the training process.

Early Stopping. Another callback in the network is the early stopping during the training. If the model doesn't improve on the validation the learning phase was stopped after 30 epochs. Therefore this could be used to define the exit strategy in the learning procedure, which is better than setting an estimated maximum epoch.

Batch Size. For performance reasons, it is recommended to choose a size that perfectly fits in the target GPU. For the setup with a TITAN RTX graphics card (24 GB) and the patch size specified in chapter 2.2.1, a range between 16 and 32 should be used. The perfect size for our setup after trying different values was 20. A value, which can be divided by 2 is recommended. The main reason is that the number of physical processors in GPUs often has a power of 2 distribution, which enables perfect pluralism when the batch size has been chosen in this type of set [11].

2.3 Multi-Class Evaluation

Metrics. The metric collection framework, MISeval, was used to evaluate the trained model [12]. This enables to calculate out of the box the F1-Score, Accuracy and more. The basis of the calculation is the confusion matrix from the comparison of the model prediction and the ground truth of our test sample. All results are saved in a separate file, which is used to create our boxplot representation.

Table 2.1: Description of all used metrics with their calculation formula and general interpretation in the context of model evaluations. TP - true positive, TN - true negative, FP - false positive, FN - false negative. [12]

Metric	Formula	Interpretation
F1-score	$DSC = \frac{2TP}{2TP + FP + FN}$	Average score of precision and recall metric.
Accuracy	$ACC = \frac{TP + TN}{TP + TN + FN + FP}$	Ratio of correctly predicted observation to the total amount of predictions.
AUC	$AUC = 1 - \frac{1}{2} \left(\frac{FP}{FP + TN} + \frac{FN}{FN + TP} \right)$	Aggregate measure of all classification thresholds from the ROC Curve. Probability that the model ranks a random positive example more highly than a random negative example.
IoU	$IoU = \frac{TP}{TP + FP + FN}$	Amount of overlap between the predicted and the ground truth observation.
MCC	$MCC = \frac{TP * TN - FP * FN}{\sqrt{(TP + FP)(FP + FN)(TN + FP)(TN + FN)}}$	High Score only if good results in all four confusion matrix categories.

Visualizations. For every metric, a boxplot was created with the seaborn framework, which visualizes the test sample values for every class separately [13]. In addition, a mean value over all samples is calculated. To evaluate the model, a routine was implemented to create a segmented image, which combines the origin tile and the predicted mask for selected samples. During the learning process, a live visualization of the progress is possible through the TensorBoard extension [14]. In order to make the respective web interface accessible, the pipeline calls a separate startup and callback function for each execution.

Pipeline extensions. MIScnn has already supported us to create a pipeline that automates the process from preprocessing throw the learning to the final evaluation. For this work, the pipeline was been extended to apply different configurations with a single function call. These configurations featured different loss functions, datasets, superclasses, data splits, batch sizes and more. There also create a matched folder structure and save all important data, which was discussed earlier. The complete source code is accessible throw the GitHub platform [15].

3 Results and Discussion

Emerging Data Challenges. The Data Exploration reveals that the datasets contain many inaccurate bounding boxes which have a negative impact on the evaluation task. Another problem is very rare classes and the superclass "other" (Section 2.1). To avoid extreme class imbalances and evaluation problems, these classes did not get a separate superclass and therefore these classes are integrated into the FOV area. The

previous test attempts to include the "other"-class with the MIScnn Framework were not successful. The NuCLS study models also exclude the "other"-class from their metric analysis. Further, the samples were taken from different device types in different clinical environments. This could lead to differences in quality or unwanted influences of device characteristics on the samples. In the worst case, the model learns these peculiarities from the different recording devices, which could also have a negative impact on our scores. The NuCLS study even reinforced this problem by sorting the samples according to the devices and building per device a fold set. This approach is bypassed in this study by using a percentage split and shuffling the complete dataset before every training (Section 2.2.1).

Segmentation Performance. Three models were created for the three different datasets discussed in Section 2.1. After around 40 - 60 epochs the training progress began to converge and no longer improved significantly. After 100 - 150 epochs the TensorFlow callback exit the training phase. The individual results of the three model evaluations are summarized and interpreted in the following sections. All scores have been rounded to one decimal place and are normalized between the range 0 to 100.

Single-rater Dataset. A large evaluation dataset with 347 samples was analyzed. This is important because the single-rater dataset has low quality annotations. A large ground truth base could compensate for possible erroneous annotations. The stromal class did not perform well in comparison to the other classes. Tumor and sTILs were able to achieve relatively good results if the outliers with a zero score were disregarded.

Table 3.1: Scores of the single-rater dataset model and a 60-20-20 cross-validation with shuffled samples.

Class	MCC	IoU	ACC	AUC	F1
FOV	59.2	80.8	84.8	79.7	89.4
Tumor	59.1	50.9	85.2	80.5	67.4
Stromal	25.0	11.2	93.4	56.1	20.2
sTILs	54.1	40.2	94.6	79.8	57.3
∅	47.7	49.2	88.0	73.6	60.0

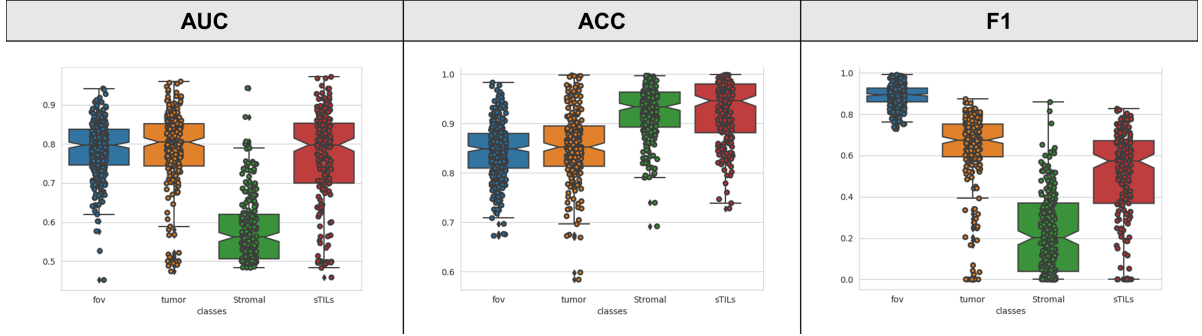


Figure 3.1: Boxplot representation of the AUC, ACC and F1 metrics from the single-rater dataset results.

Single-rater Dataset & Multi-rater Dataset. This model is trained and validated with 1744 single-rater samples and evaluated with a small set of 53 high quality annotations. The model performs in all categories better than the exclusive single-rater dataset. Stromal’s score even doubled in the F1, MCC and IoC categories. This leads to the assumption that high quality annotation is very important, especially in the evaluation. These cannot be compensated by a higher number of samples of poorer quality.

Table 3.2: Single & multi-rater model results. 1257 samples for training (low quality), 485 for validation (low quality), 53 for evaluation (high quality).

Class	MCC	IoU	ACC	AUC	F1
FOV	55.8	83.1	85.3	78.2	90.7
Tumor	59.5	52.9	88.8	79.7	69.2
Stromal	40.5	29.4	92.4	68.7	45.5
sTILs	55.4	38.9	95.8	77.3	56.0
\emptyset	51.2	51.4	89.7	75.9	63.8

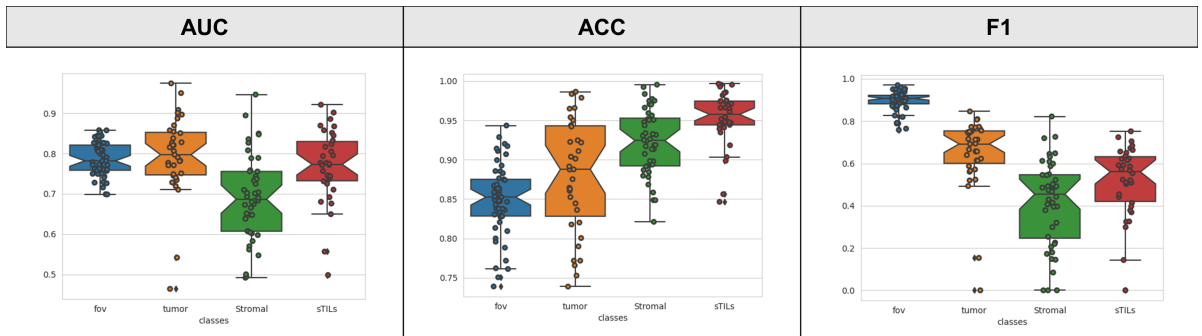


Figure 3.2: Boxplot representation of the AUC, ACC & F1 metrics from the single & multi-rater results.

Single-rater Dataset without Bounding Boxes. All bounding boxes are removed without a replacement for the training. The idea was to strengthen the annotations with good quality. Unfortunately, the bounding boxes made up too much of the annotations. This resulted in a model that could hardly classify the data. The approach is therefore not effective and can be discarded. Another idea could be not to remove the annotations but reduce the class weight for the individual annotation.

Table 3.3: Single-rater results without bounding boxes. This approach could not classify our task correctly.

Class	MCC	IoU	ACC	AUC	F1
FOV	5.7	79.2	79.5	50.2	88.4
Tumor	0.0	0.0	82.2	50.0	0.0
Stromal	0.0	0.0	92.1	50.0	0.0
sTILs	29.0	11.0	96.3	55.8	19.8
\emptyset	7.8	27.1	85.4	51.8	31.8

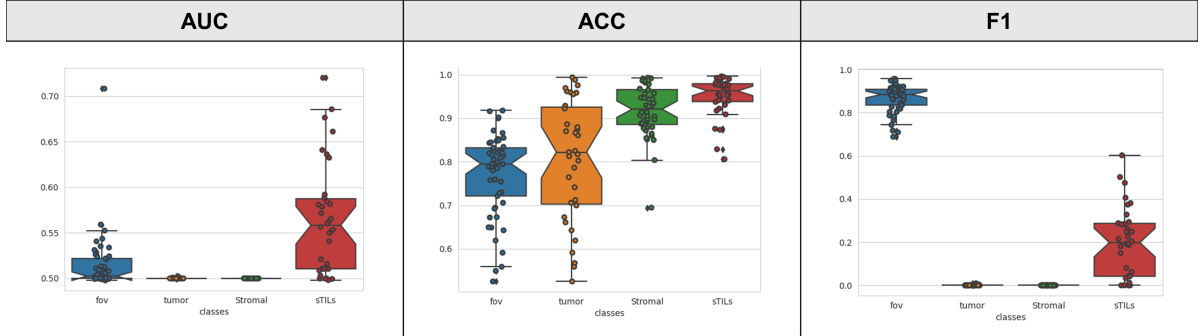


Figure 3.3: Boxplot representation of the AUC, ACC & F1 metrics. Single-rater results without bounding boxes.

Comparison between the NuCLS and MaskRCNN Models. The NuCLS study provides a strongly customized model for their Dataset. They also trained a model with a general MaskRCNN [16]. Both models are trained, validate and evaluate with the single-rater dataset. Both results should now be compared directly with our previous single-rater result.

Table 3.4: Direct comparison of the different models. Customized model from NuCLS (r.), standard MaskRCNN (m.), our results (r.). The NuCLS and MaskRCNN model evaluation have slightly different metrics. So some information is missing and is left out in the table.

	NuCLS models			MaskRCNN			our results			
Class	MCC	ACC	AUC	MCC	ACC	F1-Score	MCC	ACC	AUC	F1-Score
Tumor	71.7	-	94.2	63.0	83.2	74.9	59.2	84.8	79.7	89.4
Stromal	49.4	-	85.4	26.3	82.2	17.5	59.1	85.2	80.5	67.4
sTILs	73.5	-	94.7	58.1	75.5	77.4	25.0	93.4	56.1	20.2
other	-	-	-	12.0	97.9	11.9	-	-	-	-
Overall	65.6	77.7	86.0	52.7	69.1	-	47.7	88.0	73.6	60.0

The standard MaskRCNN results are slightly worse or equal to our MIScnn Network. The NuCLS model outperforms the other standard networks. But it is important to note that the NuCLS model uses a k-fold cross-validation, which is sorted by device and recording sessions. This has a positive impact on the evaluation that should not be underestimated. This NuCLS network is also highly customized to the specific task.

Limitation. The single-rater model and the combination model provided solid results for the task of tumor classification of cell nuclei. Our approach to eliminating all bounding boxes did not lead to good results. A solution might be to not eliminate the bounding boxes completely, but only to adjust their weight per instance. MIScnn is currently not sufficiently adapted for multiclass problems. Only class weights can be applied globally across all samples. A better approach would be if the weights could be calculated and set per sample or coordinate. But also with adjustments of the weights is the partial annotation with bounding boxes a limitation. A more precise annotation, especially in the multi-rater dataset, would be beneficial. The hybrid annotations types have a negative impact on the evaluation phase, which should not be underestimated. To further strengthen our model, specific adjustments to our pipeline are needed to better meet the task of cell nucleus segmentation. For example the usage of class probability vectors or increasing the density of region proposals, which both are present in the NuCLS study. Another important aspect is the data augmentation, which was performed in Chapter 2.2.1. These modifications should be used carefully and can be further adapted to the cell nucleus samples. A modification per recording device may also be useful to adapt the data sources to one another as far as possible. In the course of this, the samples could also be converted to a uniform size so that padding and strides methods do not influence the result. In order to further customize the model specifically to the problem, more research is generally required in the domain of cell nuclei and their particularities.

4 Conclusion

Our short study showed that with a generic u-net architecture and the MIScnn pipeline, we achieved slightly moderate to good results in the multi-class classification of cell nuclei. The MIScnn framework makes it efficient to create initial test runs for complex models in order to approach the task. However, the created models cannot fully reach the level of an extended and adapted approach such as the NuCLS model. Nevertheless, it can be a first step in the development of these. After further extensive adjustments, the level of the NuCLS study should be reached, especially with regard to the mentioned sorted cross-validation. MIScnn provides mature and general templates for tackling a wide range of complex problems with an efficient collection of functions.

Appendix

The code for this article was implemented in Python (platform independent) and is available under the GPL-3.0 License at the following GitHub repository: <https://github.com/Pfleiderer-Adrian/NuCLS.MIScnn>.

References

- [1] M. Amgad and Atteya, *Nucls: A scalable crowdsourcing, deep learning approach and dataset for nucleus classification, localization and segmentation*, 2021. DOI: 10.48550/ARXIV.2102.09099.
- [2] *Tcga-brca study*, 2016. [Online]. Available: <https://portal.gdc.cancer.gov/projects/TCGA-BRCA> (visited on 04/16/2022).
- [3] *National cancer institute*. [Online]. Available: <https://www.cancer.gov/> (visited on 04/20/2022).
- [4] D. Müller and F. Kramer, “Miscnn: A framework for medical image segmentation with convolutional neural networks and deep learning,” *BMC Medical Imaging*, vol. 21, 2021. DOI: 10.1186/s12880-020-00543-7.
- [5] *TensorFlow: Large-scale machine learning on heterogeneous systems*, Software available from tensorflow.org, 2015. [Online]. Available: <https://www.tensorflow.org/>.

- [6] D. Müller, I. Soto-Rey, and F. Kramer, “Robust chest ct image segmentation of covid-19 lung infection based on limited data,” *Informatics in Medicine Unlocked*, vol. 25, 2021, ISSN: 2352-9148. DOI: <https://doi.org/10.1016/j.imu.2021.100681>.
- [7] O. Ronneberger, P. Fischer, and T. Brox, “U-net: Convolutional networks for biomedical image segmentation,” *CoRR*, vol. abs/1505.04597, 2015. arXiv: 1505.04597. [Online]. Available: <http://arxiv.org/abs/1505.04597>.
- [8] T.-Y. Lin, P. Goyal, R. Girshick, K. He, and P. Dollar, *Focal Loss for Dense Object Detection*. Oct. 2017.
- [9] G. King and L. Zeng, “Logistic regression in rare events data,” *Political Analysis*, vol. 9, 137–163, Spring 2001.
- [10] F. Pedregosa, G. Varoquaux, and G. et al., “Scikit-learn: Machine learning in Python,” *Journal of Machine Learning Research*, vol. 12, pp. 2825–2830, 2011.
- [11] M. J. Flynn, “Some computer organizations and their effectiveness,” *IEEE Transactions on Computers*, vol. C-21, no. 9, pp. 948–960, 1972.
- [12] D. Müller, D. Hartmann, P. Meyer, F. Auer, I. Soto-Rey, and F. Kramer, *Miseval: A metric library for medical image segmentation evaluation*, Jan. 2022.
- [13] M. L. Waskom, “Seaborn: Statistical data visualization,” *Journal of Open Source Software*, vol. 6, no. 60, p. 3021, 2021. DOI: 10.21105/joss.03021.
- [14] *TensorBoard: Tensorflow’s visualization toolkit*, Software available from tensorflow.org, 2015. [Online]. Available: <https://www.tensorflow.org/tensorboard>.
- [15] *Github repository for nucleus segmentation and analysis*. [Online]. Available: <https://github.com/Pfleiderer-Adrian> (visited on 04/30/2022).
- [16] K. He, G. Gkioxari, P. Dollár, and R. Girshick, “Mask r-cnn,” in *2017 IEEE International Conference on Computer Vision (ICCV)*. DOI: 10.1109/ICCV.2017.322.